

3D Semi-Supervised Learning with Uncertainty-Aware Multi-View Co-Training

Yingda Xia¹, Fengze Liu¹, Dong Yang², Jinzheng Cai³, Lequan Yu⁴,
Zhuotun Zhu¹, Daguang Xu², Alan Yuille¹, Holger Roth²

¹Johns Hopkins University ²NVIDIA Corporation

³University of Florida ⁴The Chinese University of Hong Kong

Abstract

We propose a novel framework, **uncertainty-aware multi-view co-training (UMCT)**, to address semi-supervised learning on 3D data, such as volumetric data in medical imaging. The original co-training method was applied to non-visual data. It requires different sources, or representations, of the data, which are called different views and differ from viewpoint in computer vision. Co-training was recently applied to visual tasks where views were deep networks learnt by adversarial training. In our work, targeted at 3D data, co-training is achieved by exploiting multi-viewpoint consistency. We generate different views by rotating the 3D data and utilize asymmetrical 3D kernels to further encourage diversified features of each sub-net. In addition, we propose an uncertainty-aware attention mechanism to estimate the reliability of each view prediction with Bayesian deep learning. As one view requires the supervision from other views in co-training, our self-adaptive approach computes a confidence score for the prediction of each unlabeled sample, in order to assign a reliable pseudo label and thus achieve better performance. We show the effectiveness of our proposed method on several open datasets from medical image segmentation tasks (NIH pancreas & LiTS liver tumor dataset). A method based on our approach achieved the state-of-the-art performances on both the LiTS liver tumor segmentation and the Medical Segmentation Decathlon (MSD) challenge, demonstrating the robustness and value of our framework even when fully supervised training is feasible.

1. Introduction

Deep learning has achieved great successes in various computer vision tasks, such as 2D image recognition [20, 35, 36, 15, 17] and semantic segmentation [25, 7, 40, 8]. However, deep networks usually rely on large-scale labeled datasets to train on. When it comes to 3D data, such as

medical volumetric data and point clouds, human labeling can be extremely costly. Take medical imaging for example, with the rapid growth in the demand of finer and larger scale of Computer Aided Diagnoses (CAD), 3D segmentation of medical images (such as CTs and MRIs) is acting as a critical step in biomedical image analysis and surgical planning. But well-annotated segmentation labels in medical images require high-level expertise of radiologists and careful manual labeling on the contours and boundaries. Therefore, semi-supervised approaches with unlabeled data occupying a large portion of the training data are worth exploring especially in this targeted field.

In this paper, we aim to design a semi-supervised approach for 3D data, which can be applied to diverse data sources, e.g. CT/MRI volumes, image sequences and 3D point clouds. Inspired by the success of [5] and its extension into single 2D images [29], we further extend this idea into 3D. Typical co-training requires at least two views (i.e. sources) of data, either is sufficient to train a classifier on, and minimizes the disagreements by assigning pseudo labels to each other on unlabeled data. Blum and Mitchell [5] further proved that co-training has PAC-like guarantees on semi-supervised learning with an additional assumption that the two views are conditionally independent given the category. Since most computer vision tasks have only one source of data, encouraging view differences is a crucial point for successful co-training. Deep co-training [29] trains multiple deep networks to act as different views by utilizing adversarial examples [14] to address this issue. Another aspect we want to emphasize is view confidence estimation. In multi-view settings, given sufficient variance of each view, the quality of each prediction is not guaranteed and bad pseudo labels can be harmful for the training procedure. Co-training will benefit from trusting the reliable predictions and degrading the unreliable ones. However, distinguishing reliable from unreliable predictions is challenging because we need to evaluate on unlabeled data without ground-truth.

To address the above two important aspects, we propose

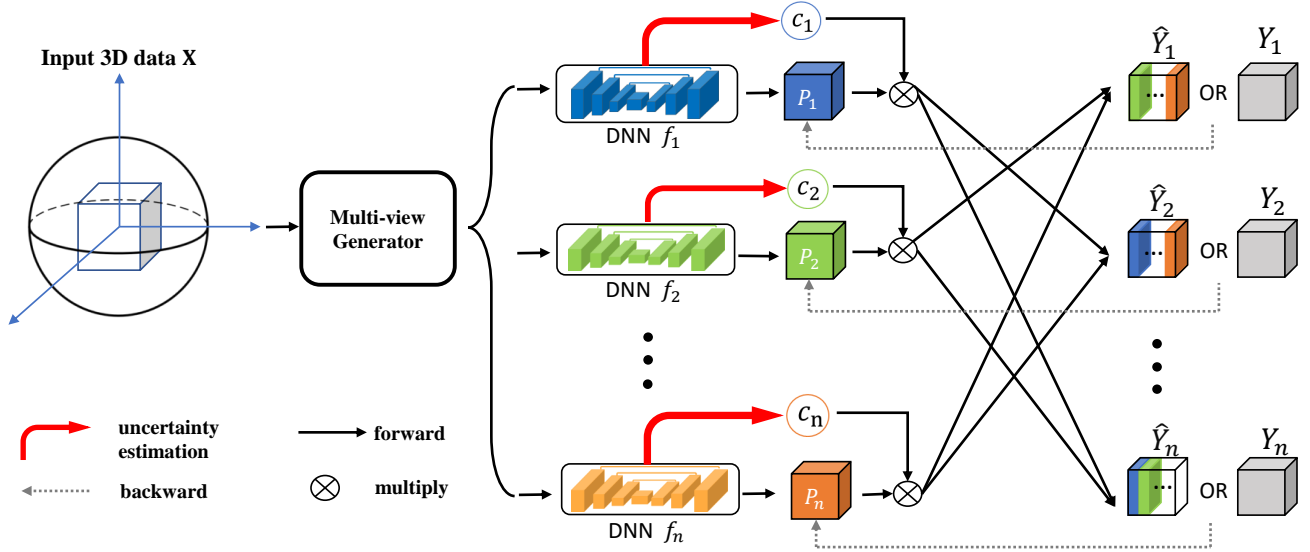


Figure 1: Overall framework of UMCT (best viewed in color). We first generate multi-view inputs of \mathbf{X} and forward into n deep networks. A confidence score c is computed for each view by uncertainty estimation, and acts as an attention weight to compute the pseudo labels (\hat{Y}) of other views. We then use these pseudo labels as supervision for unlabeled data to train the deep networks, while we only use the groundtruth (Y) for labeled data.

uncertainty-aware multi-view co-training (UMCT) framework. First of all, we define the concept of “view” in our work as a data-model combination which combines the concepts of data source (classical co-training) and deep network model (deep co-training). Although only one source of data is available, we can still introduce data-level view differences by exploring multiple viewpoints of 3D data through spatial transformations, such as rotation and permutation. Hence, our multi-view approach naturally adapts to analyze 3D data, and can be integrated with our proposed co-training framework.

We further introduce model-level view differences. We propose to adopt 2D initialized models with asymmetric kernels in three dimensions, such as $3 \times 3 \times 1$ kernels. In this way, we can not only utilize the existence of 2D pre-trained models, but also train the whole framework in a full 3D fashion [24]. Such design also introduces 2D biases in each view during training, leading to complementary feature representations in the different views. During the training process of UMCT, we minimize this disagreements of views through 3D co-training, which will further boost the performance of our model.

Another component of UMCT is view confidence estimation. We propose to estimate the uncertainty of each view prediction with Bayesian deep networks by adding dropout into our architectures [13]. We compute a confidence score based on epistemic uncertainty [19], which can act as an attention mechanism for each prediction. After propagation through this *uncertainty-aware attention mod-*

ule (UAM), a set of more accurate pseudo labels can be obtained for each view, which leads to improved co-training.

Thus, “multi-view” in UMCT contains a two-fold meaning: one is ‘multi-view learning’ [38] as known in machine learning literature; the other is ‘multi-viewpoint analysis’ of 3D data as common in computer vision. We evaluate our approach on the NIH pancreas segmentation dataset and the training/validation set of LiTS liver tumor segmentation challenge, outperforming other semi-supervised methods by a large margin. We further investigate the influence of UMCT when applying it in a fully supervised setting, to see whether it also assists training for each branch with sufficient labeled data. A method based on our approach achieved the state-of-the-art results on LiTS liver tumor segmentation challenge and scored the second place in the Medical Segmentation Decathlon challenge, without using complicated data augmentation or model ensembles.

2. Related Work

Semi-supervised learning Semi-supervised learning approaches aim at learning models with limited labeled data and a large proportion of unlabeled data [5, 44, 3, 43]. Emerging semi-supervised approaches have been successfully applied to image recognition using deep neural networks [21, 31, 27, 1, 34]. These algorithms are mostly based on adding regularization terms to train networks to be resistant to some specific noise. A recent approach [29] extended the co-training strategy to 2D deep networks and multiple views, using adversarial examples to encour-

age view differences to boost performance. Tri-Net [11] trains a three-branch network to supervise each other, which can also be viewed as a multi-view learning [38] approach that encourages view differences with classifiers of diverse structures.

Semi-supervised medical image analysis [9] mentioned that current semi-supervised medical analysis methods fall into 3 types - self-training (teacher-student models), co-training (with hand-crafted features) and graph-based approaches (mostly applications of graph-cut optimization). [2] introduced a deep network based self-training framework with conditional random field (CRF) based iterative refinements for medical image segmentation. [41] trained three 2D networks from three planar slices of the 3D data and fused them in each self-training iteration to get a stronger student model. [23] extended the self-ensemble approach π model [21] with 90 degree rotations making the network rotation-invariant. GAN based approaches are also popular recently for medical imaging [10, 18, 28].

Uncertainty Estimation Traditional approaches include particle filtering and CRFs [4, 16]. For deep learning, uncertainty are more often measured with Bayesian deep networks [13, 12, 19]. In our work, we stress the importance of uncertainty estimation in semi-supervised learning, since most of the training data here is not annotated. We propose to estimate the confidence of each view in our co-training framework via Bayesian uncertainty estimation.

2D/3D hybrid networks 2D networks and 3D networks both have their advantages and limitations. The former benefit from 2D pre-trained weights and well-studies architectures in natural image processing, while the latter better explore 3D information utilizing 3D convolutional kernels. [37, 22] either uses 2D probability maps or 2D feature maps for building 3D models. [24] proposed a 3D architecture which can be initialized by 2D pre-trained models. Moreover, [33, 42] illustrates the effectiveness of multi-view training on 2D slices, even by simply averaging multiplanar results, indicating complementary latent information exists in the biases of 2D networks. This inspired us to train 3D multi-view networks with 2D initializations jointly using an additional loss function for multi-view networks, encouraging each network to learn from each other.

3. Uncertainty-aware Multi-view Co-training

In this section, we introduce our framework of *uncertainty-aware multi-view co-training* (UMCT). We mentioned two important properties for a successful deep network based co-training: view difference and view reliability. Here, we will explain how we achieve these properties in our 3D setting. We firstly give a general mathematical formulation of the approach in Sec 3.1, and then introduce how to compute the confidence of each view by

uncertainty estimation in Sec 3.2. Finally, we apply our approach to 3D medical image segmentation, and study task-dependent settings in Sec 3.3.

3.1. Overall Framework

We consider the task of semi-supervised learning for 3D data. Let \mathcal{S} and \mathcal{U} be the labeled and unlabeled dataset, respectively. Let $\mathcal{D} = \mathcal{S} \cup \mathcal{U}$ be the whole provided dataset. We denote each labeled data pair as $(\mathbf{X}, \mathbf{Y}) \in \mathcal{S}$ and unlabeled data as $\mathbf{X} \in \mathcal{U}$. The ground truth \mathbf{Y} can either be a ground truth label (classification tasks) or dense prediction map (segmentation tasks).

Suppose for each input \mathbf{X} , we have N views denoted as $v_i(\cdot)$, $i = 1, \dots, N$. We can naturally generate different views of 3D data by rotating it into multiple viewpoints. Such operation will introduce a data-level view difference. We then train N models $f_i(\cdot)$, $i = 1, \dots, N$ over each view of data. If $(\mathbf{X}, \mathbf{Y}) \in \mathcal{S}$, then we optimize a supervised loss function \mathcal{L}_{sup} , measuring the similarity between the prediction of each view (data-model combination) $p_i(\mathbf{X}) = f_i(v_i(\mathbf{X}))$ and \mathbf{Y} as

$$\mathcal{L}_{sup}(\mathbf{X}, \mathbf{Y}) = \sum_{i=1}^N \mathcal{L}(p_i(\mathbf{X}), \mathbf{Y}), \quad (1)$$

where \mathcal{L} is a standard loss function for a supervised learning task (e.g. classification, or segmentation).

We then construct the co-training assumption in our semi-supervised setting. The co-training strategy assumes the prediction on each view should reach a consensus. So the prediction of each model can act as a pseudo label to supervise other views in order to learn from unlabeled data. Since we expect the prediction of each view to be diverse after boosting view differences, the confidence of each view needs to be measured before generating trustworthy pseudo labels. This part is accomplished by our *uncertainty-aware attention module* (UAM), introduced in the next subsection, and is designed for deep neural networks in our framework. With UAM, we can formulate the co-training loss in the following format:

$$\mathcal{L}_{cot}(\mathbf{X}) = \sum_i^N \mathcal{L}(p_i(\mathbf{X}), \hat{\mathbf{Y}}_i), \quad (2)$$

where

$$\hat{\mathbf{Y}}_i = U_{f_1, \dots, f_n}(p_1(\mathbf{X}), \dots, p_{i-1}(\mathbf{X}), p_{i+1}(\mathbf{X}), \dots, p_n(\mathbf{X})) \quad (3)$$

is the pseudo label for the i^{th} view, U_{f_1, \dots, f_n} is the UAM computational function.

Overall, we propose to optimize the following combined loss function:

$$\sum_{(\mathbf{X}, \mathbf{Y}) \in \mathcal{S}} \mathcal{L}_{sup}(\mathbf{X}, \mathbf{Y}) + \lambda_{cot} \sum_{\mathbf{X} \in \mathcal{U}} \mathcal{L}_{cot}(\mathbf{X}). \quad (4)$$

Algorithm 1 Uncertainty-aware Multi-view Co-training

Input:Labeled dataset \mathcal{S} & Unlabeled dataset \mathcal{U} Uncertainty-aware attention module (UAM) $U_{f_1, \dots, f_n}(\cdot)$ **Output:**Model of each view f_1, \dots, f_n

- 1: **while** stopping criterion not met:
 - 2: Sample batch $b_l = (x_l, y_l) \in \mathcal{S}$ and batch $b_u = (x_u) \in \mathcal{U}$
 - 3: Generate multi-view inputs $v_i(x_l)$ and $v_i(x_u)$, $i \in \{1, \dots, N\}$
 - 4: **for** i **in** all views:
 - 5: Compute predictions for each view
 $p_i(x_l) \leftarrow f_i(v_i(x_l))$, $p_i(x_u) \leftarrow f_i(v_i(x_u))$
 - 6: **for** i **in** all views:
 - 7: Compute pseudo labels for x_u with UAM
 $\hat{y}_i \leftarrow U_{f_1, \dots, f_n}(p_1(x_u), \dots, p_{i-1}(x_u), p_{i+1}(x_u), \dots, p_n(x_u))$
 - 8: $\mathcal{L}_{sup} = \frac{1}{|b_l|} \sum_{(x_l, y_l) \in b_l} [\sum_i^N \mathcal{L}(p_i(x_l), y_l)]$
 - 9: $\mathcal{L}_{cot} = \frac{1}{|b_u|} \sum_{(x_u) \in b_u} [\sum_i^N \mathcal{L}(p_i(x_u), \hat{y}_i)]$
 - 10: $\mathcal{L} = \mathcal{L}_{sup} + \lambda \mathcal{L}_{cot}$
 - 11: Compute gradient of loss function \mathcal{L} and update network parameters $\{\theta_i\}$ by back propagation
 - 12: **return** f_1, \dots, f_n
-

3.2. Uncertainty-aware Attention Module

Encouraging view difference means enlarging the variance of each view prediction $var(p_i(\mathbf{X}))$. This raises the question of which view we should trust to continue with our co-training. Bad predictions from one view may hurt the training procedure of other views through pseudo-label assignments. Meanwhile, encouraging to trust a good prediction as a “strong” label from co-training will boost the performance, and lead to an improved performance of overall semi-supervised learning. Instead of assigning a pseudo-label for each view directly from the predictions of other views, we propose an adaptive approach, namely our *uncertainty-aware attention module* (UAM), to fuse the outputs of different views. UAM is built up of all the views, takes the prediction of each view as input, and then outputs a set of pseudo labels for each view.

Motivated by the uncertainty measurements in Bayesian deep networks, we measure the uncertainty of each view branch for each training sample after turning our model into a Bayesian deep network by adding dropout layers. Between the two types of uncertainty candidates – aleatoric and epistemic uncertainties, we choose to compute the epistemic uncertainty that is raised by not having enough training data [19]. Such measurement fits the semi-supervised learning goal: to improve model generalizability by exploring unlabeled data. Suppose y is the output of a Bayesian

deep network, then the epistemic uncertainty can be estimated by the following equation:

$$U_e(y) \approx \frac{1}{T} \sum_{t=1}^T \hat{y}_t^2 - \left(\frac{1}{T} \sum_{t=1}^T \hat{y}_t \right)^2, \quad (5)$$

where $\{\hat{y}_t\}_{t=1}^T$ are a set of sampled outputs.

With a transformation function $\mathbf{h}(\cdot)$, we can transform the uncertainty score into a confidence score $\mathbf{c}(y) = \mathbf{h}(U_e(y))$. After normalization over all views, the confidence score will act as an attention weight for each prediction to assign as a pseudo label for other views. The pseudo label $\hat{\mathbf{Y}}_i$ assigned for a single view i can be formatted as

$$\hat{\mathbf{Y}}_i = \frac{\sum_{j \neq i}^N \mathbf{c}(p_j(\mathbf{X})) p_j(\mathbf{X})}{\sum_{j \neq i}^N \mathbf{c}(p_j(\mathbf{X}))}. \quad (6)$$

3.3. UMCT with asymmetric 3D models for medical segmentation

Here, we consider the specific scenario of medical image segmentation, where the input data is a 3D volume. In order to generate multi-view data, we transpose \mathbf{X} into multiple views. For three-view co-training, such these can correspond to the coronal, sagittal and axial views in medical imaging, which matches the multi-planar reformatted views that radiologists typically use to analyze the image. However, if we would simply forward these volumes into traditional 3D segmentation networks, we will possibly encounter the risk that these networks will collapse into each other, as mentioned in [29].

In order to avoid such condition, we encourage view difference at feature level by designing a task-specific model. We propose to use 2D-initialized asymmetric 3D models for the backbone network of each view to encourage diverse features for each view learning. The simplest version of an asymmetric 3D model is to use $n \times n \times 1$ convolutional kernels instead of $n \times n \times n$ 3D kernels in common 3D networks. This structure also makes the model convenient to be initialized with 2D pre-trained weights and fine-tuned in a 3D fashion. Such a backbone design gives us two-fold benefits. One is the whole model can benefit from 2D pre-trained weights for better feature learning. The other is that the intrinsic asymmetric structure prevents multi-view networks from collapsing into each other and provides complementary information.

Hence, we forward the rotated volumes into such deep networks $\{f_i(\cdot)\}_{i=1}^N$ with parameters $\{\theta_i\}_{i=1}^N$ and rotate the outputs of the networks back to align them into a common view. $\{p_i(\mathbf{X})\}_{i=1}^N$ are the corresponding voxel-wise prediction score maps:

$$p_i(\mathbf{X}) = T_i^{-1}(f_i(T_i(\mathbf{X}); \theta_i)), \quad (7)$$

where T_i denotes the i^{th} rotation operation to generate multi-view inputs. On the supervised dataset \mathcal{S} , each \mathbf{X} has a ground truth voxel-wise label \mathbf{Y} . For each of the single-view sub-network, we use Dice loss [26] as the training objective, which is defined as,

$$\mathcal{L}_{Dice} = 1 - \frac{2 \sum_{i=1}^N y_i \hat{y}_i}{\sum_{i=1}^N y_i^2 + \sum_{i=1}^N \hat{y}_i^2}, \quad (8)$$

where y_i and \hat{y}_i represent the ground truth label and the network prediction, respectively. The Dice loss performs robustly with imbalanced training data. More importantly, we use the Dice loss to mitigate the gap between the training objective and commonly used evaluation metrics, such as Dice score.

In terms of view confidence estimation, we modify the network into a Bayesian deep network by adding dropout operations. We sample $T = 10$ outputs for each view and compute voxel-wise epistemic uncertainty. Since the voxel-wise uncertainty can be inaccurate, we sum over the whole volume to finalize the uncertainty for each view. We simply use the reciprocal for the confidence transformation function $\mathbf{h}(\cdot)$ to compute the confidence score. The pseudo label assigned for one view is a weighted average of all predictions of multiple views based on the normalized confidence score. After obtaining the pseudo label set $\{\hat{\mathbf{Y}}_i\}_{i=1}^N$ from Eqn. (3), we can optimize the network parameters $\{\theta_i\}_{i=1}^N$ according to Eqn. (1)(2)(4).

Note that we only minimize co-training loss on the unlabeled data. As we already optimize the Dice loss on the supervised data to force the network prediction to be close to the ground truth, we do not need to enforce the co-training assumption again under such semi-supervised settings. However, we will later show that the co-training loss can also help each branch to learn better features on labeled data. But under semi-supervised settings, this improvement is negligible concerned with the limited labeled data we have. The overall framework is described in Figure 1.

In the training phase, we try to optimize Eqn. (4) by gradient descent. For each iteration, we sample a labeled batch $b_l = (x_l, y_l)$ and an unlabeled batch $b_u = (x_u)$. We first compute gradients based on Eqn. (1) after forwarding the labeled batch and then aggregate gradients after forwarding the gradients from the unlabeled loss based on Eqn. (2). We update parameters at the end of each iteration. The training algorithm is shown in Algorithm 1.

In the testing phase, we have two choices to finalize the output results - either to choose one single view prediction or to ensemble the predictions of the multi-view outputs. We will report both results in the next sections for fair comparison with the baselines, because the multiple view networks can be thought of being similar to the ensemble of several single view models. We will show in experiments

that our model improves the performance in both settings (single view and multi-view ensemble).

3.4. Implementation Details

Network Structure In practice, we build an encoder-decoder network based on ResNet-18[15], and modified it into a 3D version. For encoder part, the first 7×7 convolutional layer is inflated into $7 \times 7 \times 7$ kernels for low level 3D feature extraction. All other 3×3 convolutional layers are simply changed into $3 \times 3 \times 1$ that can be trained in as a 3D convolutional layer. In the decoder part, we adopt 3 skip connections from the encoder followed by 3D convolutions to give low level cues for more accurate boundary prediction needed in segmentation tasks.

Data Pre-processing All the training and testing data are firstly re-sampled to an isotropic volume resolution of 1.0 mm for each axis. Data intensities are normalized to have zero mean and unit variance. We adopt patch-based training, and sample training patches of size 96^3 with 1:1 ratio between foreground and background. Unlike other 3D segmentation approaches, we do not rely on any kind of 3D data augmentation due to the effectiveness of initialization with 2D pre-trained weights.

Training We firstly train the views separately on the labeled data, and then conduct UMCT by fine-tuning the weights. We use the stochastic gradient descent (SGD) optimizer for both stages. In the view-wise training stage, we adopt a constant learning rate policy at 7×10^{-3} , momentum at 0.9 and weight decay of 4×10^{-5} for 20k iterations. In the co-training stage, we adopt a constant learning rate policy at 1×10^{-3} , with the parameter $\lambda_{cot} = 0.2$ and train for 5k iterations. The batch size is 4 for both stages. We implement our framework in PyTorch. The whole training procedure takes ~ 12 hours on 4 NVIDIA Titan V GPUs.

Testing In the testing phase, we follow a coarse-to-fine strategy using a sliding window approach [45]. In order to reduce the inference time, we first employ a coarse stride of 48 and then a fine stride of 16, using the same size patch and resolution as in training. Then we re-sample our testing results back to the original image resolution to obtain the final results. Testing time for each case ranges from 1 minute to 5 minutes depending on the size of the input volume.

4. Experiments

In this section, we give the experimental results on two popular organ segmentation datasets: NIH pancreas segmentation datasets [32] and LiTS liver tumor segmentation dataset under semi-supervised settings. Moreover, noticing that UMCT is also applicable to fully-supervised settings, we apply UMCT to supervised training and show the benefits even when all the training data is labeled.

Method	Backbone	10% lab	20% lab
Supervised	3D ResNet-18	66.75	75.79
DMPCT [41]	2D ResNet-101	63.45	66.75
DCT [29] (2v)	3D ResNet-18	71.43	77.54
TCSE [23]	3D ResNet-18	73.87	76.46
Ours (2 views)	3D ResNet-18	75.63	79.77
Ours (3 views)	3D ResNet-18	77.55	80.14
Ours (6 views)	3D ResNet-18	77.87	80.35

Table 1: Comparison to other semi-supervised approaches on NIH dataset (DSC, %). Note that we use the same backbone network as [23] [29] (“2v” means two views) and only compare the result of one single view (not multi-view ensemble) for fair comparison. “10% lab” and “20% lab” mean the percentage of labeled data used for training.

4.1. Semi-supervised segmentation

4.1.1 NIH Pancreas Segmentation Dataset

NIH pancreas segmentation dataset contains 82 abdominal CT volumes. The width and height of each volume are 512, while the axial view slice number can vary from 181 to 466. Under our semi-supervised settings, we randomly separate the dataset into 20 testing cases and 62 training cases. We report the results of 10% labeled training cases (6 labeled and 56 unlabeled), 20% labeled training cases (12 labeled and 50 unlabeled) and 100% labeled training cases. In our results, we report the performance of one single view (the average DSC score of all single views) for fair comparison, not multi-view ensemble. See Table 1.

We evaluate the segmentation accuracy by Dice-Sørensen coefficient (DSC). We notice a large margin improvement over the fully supervised baselines, in terms of single view performance, proving that our UMCT effectively explores the unlabeled data. In Fig. 2, we visualize of the worst case in the 20 testing cases in supervised training where UMCT brings an improvement of 26% in DSC. In addition, we compare our model with the state-of-the-art semi-supervised approach deep Co-training [29] and recent semi-supervised medical segmentation approaches. [23] extended π model [21] with transformation consistent constraints. [41] extended the self-training procedure, iteratively updating pseudo labels on unlabeled data by fusing three 2D networks trained on cross-sectional views. The results reported in Tab. 1 are based on our careful re-implementations in order to allow a fair comparison.

For [29] and [23], we operate on the axial view of our single view branch with the same backbone structure (our customized 3D ResNet-18 model). Our results achieve about 4% gain in the 10% labeled and 90% unlabeled settings. We also find that improvements of other approaches are small in the 20% settings (only 1% compared to the

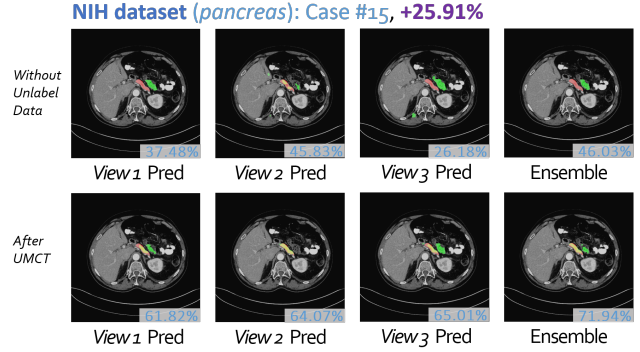


Figure 2: The visualization for the worst case in the test set in supervised training (but largely improved by UMCT). In each picture, red, green and yellow indicate ground-truth, prediction and overlap. Best viewed in color.

baseline), while ours still is capable to achieve a reasonable performance gain with the growing number of labeled data. For [41], a 2D approach, their experiment is conducted on 50 labeled cases. We modify their backbone network (FCN [25]) into DeepLab v2 [7], in order to fit our stricter settings (6 and 12 labeled cases). This modification leads to an improvement of 3% in 100% fully supervised training (from 73% to 76%). Their approach outputs the result after using an ensemble of three models.

Since the main difference in two-view learning between our approach and [29] is the way of encouraging view differences, our results illustrate the effectiveness of our multi-view analysis combined with asymmetric feature learning on 3D co-training. With more views, our UAM can further improve co-training performance. We will report ablation studies on UAM in section 4.3.

4.1.2 LiTS Liver Tumor Segmentation Challenge

We also report our results on the train validation set of LiTS Liver Tumor Segmentation Challenge. We randomly separate the 131 cases into a semi-supervised training set which contains 100 cases and test our method on the remaining 31 cases. The input volumes are all abdomen CT scans. The segmentation target contains 2 classes: liver (large and easy) and lesion (tumor with large variance in size, more challenging). Our semi-supervised settings are the same as that used in NIH pancreas dataset experiments. We report results on 10% labeled data (10 labeled cases and 90 unlabeled cases) and 20% labeled data (20 labeled case and 80 unlabeled cases) with 3-view co-training. The performance of single view and multi-view ensemble both improves. See Table 2. The improvement on liver is limited (less than 1%), because the liver segmentation is already very good. If we only use 10% data for supervised training, we can already reach 93.17% after fusing the three view results by major-

Method	Liver		Lesion	
	Single	MV	Single	MV
100% Supervised	95.07	95.50	64.00	65.65
10% Supervised	92.23	93.17	43.98	48.90
20% Supervised	93.06	94.52	50.39	53.15
UMCT 10%	92.98	93.53	49.79	52.14
UMCT 20%	94.40	94.81	57.76	59.60

Table 2: 3-view UMCT on LiTS train/val dataset (DSC, %). “Single” means the DSC score of one single view, while “MV” means multi-view ensemble. The first three rows are our fully supervised baselines. The last two rows are the results of our approach, with 10% labeled data and 20% labeled data. We report both liver and lesion (tumor) results. The improvements using UMCT over the corresponding baselines are significant, especially for the performance on liver lesions.

Method	Liver	Lesion
3D AH-Net [24]	96.3	63.4
H-DenseUNet [22]	96.1	72.2
3 views UMCT (ours)	95.9	72.6

Table 3: Results of fully supervised training with UMCT on LiTS test set (DSC, %).

ity voting. However, we see a large margin improvement in the more challenging lesion segmentation, especially under “UMCT 20%” settings (even more than “UMCT 10%”). We hypothesize that the case variance of lesions is larger than normal organs (pancreas, liver, etc). With only 10 cases for our labeled set, \mathcal{L}_{sup} can misguide the training procedure and introduce bias to the labeled set (known as overfitting). However, using \mathcal{L}_{cot} to explore the unlabeled part of the dataset, we can train a more robust model compared to fully supervised training using the same number of labeled cases. Overall, the improvements are significant even on the challenging liver lesion with large case variance.

4.2. Application to fully supervised settings

UMCT can also be applied to fully supervised training. On semi-supervised tasks, we do not see a clear improvement when enforcing \mathcal{L}_{cot} on labeled data because of the quantity limitation. However, when data quantity is large, we want to see if UMCT can guide each 2D-initialized branch to help each other by enforcing 3D consistency. The final framework for fully supervised training is: we firstly train three networks of different views, and then fine-tune with the following loss function:

$$\mathcal{L} = \sum_{(\mathbf{X}, \mathbf{Y}) \in \mathcal{S}} [\mathcal{L}_{sup}(\mathbf{X}, \mathbf{Y}) + \lambda \mathcal{L}_{cot}(\mathbf{X})] \quad (9)$$

Task	Class-wise DSC (%)		
Task01 Brats	67.52	45.00	68.01
Task02 Heart	92.46		
Task03 Liver	95.06	71.40	
Task04 Hippocampus	87.97	86.71	
Task05 Prostate	69.36	86.66	
Task06 Lung	52.15		
Task07 Pancreas	78.42	38.48	

Table 4: DSC scores on the first seven tasks of Medical Segmentation Challenge (some tasks have multi-class labels).

On LiTS dataset challenge, a method based on our approach achieved the state-of-the-art results in terms of tumor segmentation DSC score and comparable liver segmentation results. See Table 3.

On Medical Segmentation Decathlon challenge, a method based on our approach achieved the second place in the final testing phase. See Table 4. Without any hyper parameter change allowed, a favored model has to be generalizable and robust to various tasks. Our model can satisfy such requirements because we have the following features. First, our model, although trained in 3D patches, is initialized from 2D pre-trained models. We will further discuss the influence of 2D pre-trained models in the next section. Second, we have three views of networks and use \mathcal{L}_{cot} to help each other gaining more 3D information through the UMCT process. These two characteristics boost the robustness of our model on supervised volumetric segmentation tasks.

4.3. Ablation Studies

In this subsection, we will provide several ablation studies for each component of our proposed UMCT framework.

On the backbone network structure Our backbone selection (2D-initialized, heavily asymmetric 3D architecture) will introduce 2D biases in the training phase, while benefiting from such 2D pre-trained models. We have claimed that we can utilize the complementary information from 3-view networks while exploring the unlabeled data with UMCT. We give an ablation study on the network structure, which contains a V-Net [26], a common 3D segmentation network with all symmetrical kernels in all dimensions. Such network also shares a similar amount of parameters with our customized 3D ResNet-18. See Table 5a. Results of V-Net shows that our UMCT can be generally and successfully applied to 3D networks. Although the results of fully supervised parts are similar, our ResNet-18 outperforms V-Net by more than 1%, illustrating that our asymmetric design is better at encouraging view difference than traditional 3D deep networks.

Backbone	Params	Sup 10%	Semi 10%
VNet	9.44M	66.97	76.89
3D ResNet-18	11.79M	66.76	77.55
3D ResNet-50	27.09M	67.96	78.74

(a) Ablation studies on backbone structures (3 views UMCT).

Views	DSC(%)
2 views	75.63
3 views	76.49
3 views + UAM	77.55
6 views	76.94
6 views + UAM	77.87

(c) On UAM with difference views in training (10% labeled data, 3D ResNet-18).

λ_{cot}	DSC(%)
0.1	77.28
0.2	77.55
0.5	77.38

(d) λ_{cot} (10% labeled data, 3 views, 3D ResNet-18).

Method	Coronal	Sagittal	Axial	MV
100% Supervised	82.13	81.41	82.53	84.18
UMCT Supervised	82.61	82.35	83.44	84.61

(b) UMCT on 100% labeled data from the NIH data. The first row is pure single view training, while the second is UMCT. “Coronal”, “Sagittal” and “Axial” correspond to three views in CT scan in radiology.

Model	w/o Init	w/ Init
Deeplab-3D	76.09	80.11
Our 3D ResNet-50	78.70	82.53

(e) On the influence of initialization for 3D models. Experiments are done on axial view, NIH dataset.

Table 5: Ablation studies for UMCT on NIH dataset.

On UAM, number of views and parameter λ_{cot} UAM acts as an important role in pruning out bad predictions and keeping good ones as supervision to train other views. Table 5c gives single view result in multiple views experiments. The performance becomes better with more views. For two views, UAM is not applicable since we can only obtain one view prediction as a pseudo label for the other view. For three views and six views, UAM helps boost the performance, illustrating the effectiveness of our proposed approach for view confidence estimation. We also tried different values of λ_{cot} in Table 5d, where performance variance is not large. We choose $\lambda_{cot} = 0.2$ in our experiments.

On fully supervised training Table 5b shows how our UMCT helps with the fully supervised training on NIH dataset. The model used is our 3D ResNet-50 with 3 views co-training. Our UMCT improves the results on each single model, as well as the multi-view ensemble results.

On network initialization We address the importance of initialization for training a robust 3D model. In video recognition, a similar topic has been investigated [6, 30]. In the field of 3D segmentation, Liu et al. [24] designed a network structure which can be easily initialized from a ResNet-50 pre-trained model. This subsection provides an ablation study on the influence of initialization of 3D networks in the field of 3D segmentation, which is often neglected by previous works.

We trained two 3D ResNet-50 (in our settings) in axial view on NIH dataset with all 100% labeled data. One is with 2D initialization, and another one is trained from scratch. We also conduct similar comparison experiments with a DeepLab-3D model, where we directly change each 2D kernel of DeepLab(v2)-ResNet101 model into a 3D kernel. We initialize DeepLab-3D in the same way as [6]. Table 5e shows the comparison. Those models with

initialization perform remarkably better. Thus, we believe that initialization is significantly helpful to train 3D models for volumetric segmentation. Using weights from the pre-trained models of natural image processing is capable to benefit the learning process. Note that we did not apply any data augmentation when conducting these experiments. This illustrates that a good initialization can increase the robustness of the models even with such few training examples. It would be a promising research direction to investigate approaches on 3D network initialization or providing 3D pre-trained models on large-scale datasets.

5. Conclusion

In this paper, we presented *uncertainty-aware multi-view co-training* (UMCT), aimed at 3D semi-supervised learning. We extended dual view co-training and deep co-training on 2D images into multi-view 3D training, naturally introducing data-level view differences. We also proposed asymmetrical 3D kernels initialized from 2D pre-trained models to introduce feature-level view differences. In multi-view settings, we then built an *uncertainty-aware attention module* (UAM) to estimate the accuracy of each view prediction by Bayesian uncertainty measurement. Epistemic uncertainty was estimated after transforming our model into a Bayesian deep network by adding dropout. This module gives larger weight to more confidence predictions and further boost the performance on multi-view predictions. Experiments were performed on NIH pancreas dataset and LiTS liver tumor dataset, and outperformed other approaches by a large margin on NIH dataset. We also applied the co-training objectives on labeled data under fully supervised settings. The results were also promising, illustrating the effectiveness of such design of multi-view co-training on 2D-initialized networks.

References

- [1] P. Bachman, O. Alsharif, and D. Precup. Learning with pseudo-ensembles. In *Advances in Neural Information Processing Systems*, pages 3365–3373, 2014. 2
- [2] W. Bai, O. Oktay, M. Sinclair, H. Suzuki, M. Rajchl, G. Tarroni, B. Glocker, A. King, P. M. Matthews, and D. Rueckert. Semi-supervised learning for network-based cardiac mr image segmentation. In *International Conference on Medical Image Computing and Computer-Assisted Intervention*, pages 253–260. Springer, 2017. 3
- [3] M. Belkin, P. Niyogi, and V. Sindhwani. Manifold regularization: A geometric framework for learning from labeled and unlabeled examples. *Journal of machine learning research*, 7(Nov):2399–2434, 2006. 2
- [4] A. Blake, R. Curwen, and A. Zisserman. A framework for spatiotemporal control in the tracking of visual contours. *International Journal of Computer Vision*, 11(2):127–145, 1993. 3
- [5] A. Blum and T. Mitchell. Combining labeled and unlabeled data with co-training. In *Proceedings of the eleventh annual conference on Computational learning theory*, pages 92–100. ACM, 1998. 1, 2
- [6] J. Carreira and A. Zisserman. Quo vadis, action recognition? a new model and the kinetics dataset. In *Computer Vision and Pattern Recognition (CVPR), 2017 IEEE Conference on*, pages 4724–4733. IEEE, 2017. 8
- [7] L.-C. Chen, G. Papandreou, I. Kokkinos, K. Murphy, and A. L. Yuille. Deeplab: Semantic image segmentation with deep convolutional nets, atrous convolution, and fully connected crfs. *IEEE transactions on pattern analysis and machine intelligence*, 40(4):834–848, 2018. 1, 6
- [8] L.-C. Chen, G. Papandreou, F. Schroff, and H. Adam. Rethinking atrous convolution for semantic image segmentation. *arXiv preprint arXiv:1706.05587*, 2017. 1
- [9] V. Cheplygina, M. de Bruijne, and J. P. Pluim. Not-so-supervised: a survey of semi-supervised, multi-instance, and transfer learning in medical image analysis. *arXiv preprint arXiv:1804.06353*, 2018. 3
- [10] N. Dong, M. Kampffmeyer, X. Liang, Z. Wang, W. Dai, and E. Xing. Unsupervised domain adaptation for automatic estimation of cardiothoracic ratio. In *International Conference on Medical Image Computing and Computer-Assisted Intervention*, pages 544–552. Springer, 2018. 3
- [11] W. Dong-DongChen and Z.-H. WeiGao. Tri-net for semi-supervised deep learning. In *IJCAI*, 2018. 3
- [12] Y. Gal. Uncertainty in deep learning. *University of Cambridge*, 2016. 3
- [13] Y. Gal and Z. Ghahramani. Dropout as a bayesian approximation: Representing model uncertainty in deep learning. In *international conference on machine learning*, pages 1050–1059, 2016. 2, 3
- [14] I. Goodfellow, J. Shlens, and C. Szegedy. Explaining and harnessing adversarial examples. In *International Conference on Learning Representations*, 2015. 1
- [15] K. He, X. Zhang, S. Ren, and J. Sun. Deep residual learning for image recognition. In *CVPR*, 2016. 1, 5
- [16] X. He, R. S. Zemel, and M. Á. Carreira-Perpiñán. Multiscale conditional random fields for image labeling. In *Computer vision and pattern recognition, 2004. CVPR 2004. Proceedings of the 2004 IEEE computer society conference on*, volume 2, pages II–II. IEEE, 2004. 3
- [17] G. Huang, Z. Liu, L. Van Der Maaten, and K. Q. Weinberger. Densely connected convolutional networks. In *CVPR*, volume 1, page 3, 2017. 1
- [18] J. Jiang, Y.-C. Hu, N. Tyagi, P. Zhang, A. Rimmer, G. S. Mageras, J. O. Deasy, and H. Veeraraghavan. Tumor-aware, adversarial domain adaptation from ct to mri for lung cancer segmentation. In *International Conference on Medical Image Computing and Computer-Assisted Intervention*, pages 777–785. Springer, 2018. 3
- [19] A. Kendall and Y. Gal. What uncertainties do we need in bayesian deep learning for computer vision? In *Advances in neural information processing systems*, pages 5574–5584, 2017. 2, 3, 4
- [20] A. Krizhevsky, I. Sutskever, and G. E. Hinton. Imagenet classification with deep convolutional neural networks. In *Advances in neural information processing systems*, pages 1097–1105, 2012. 1
- [21] S. Laine and T. Aila. Temporal ensembling for semi-supervised learning. *ICLR 2017*, 2016. 2, 3, 6
- [22] X. Li, H. Chen, X. Qi, Q. Dou, C.-W. Fu, and P. A. Heng. H-denseunet: Hybrid densely connected unet for liver and liver tumor segmentation from ct volumes. *IEEE Transactions on Medical Imaging*, 2017. 3, 7
- [23] X. Li, L. Yu, H. Chen, C.-W. Fu, and P.-A. Heng. Semi-supervised skin lesion segmentation via transformation consistent self-ensembling model. *BMVC*, 2018. 3, 6
- [24] S. Liu, D. Xu, S. K. Zhou, T. Mertelmeier, J. Wicklein, A. Jerebko, S. Grbic, O. Pauly, W. Cai, and D. Comaniciu. 3d anisotropic hybrid network: Transferring convolutional features from 2d images to 3d anisotropic volumes. *MICCAI*, 2017. 2, 3, 7, 8
- [25] J. Long, E. Shelhamer, and T. Darrell. Fully convolutional networks for semantic segmentation. In *Proceedings of the IEEE conference on computer vision and pattern recognition*, pages 3431–3440, 2015. 1, 6
- [26] F. Milletari, N. Navab, and S.-A. Ahmadi. V-net: Fully convolutional neural networks for volumetric medical image segmentation. In *3DV*, 2016. 5, 7
- [27] T. Miyato, S.-i. Maeda, S. Ishii, and M. Koyama. Virtual adversarial training: a regularization method for supervised and semi-supervised learning. *IEEE transactions on pattern analysis and machine intelligence*, 2018. 2
- [28] D. Nie, Y. Gao, L. Wang, and D. Shen. Asdnet: Attention based semi-supervised deep networks for medical image segmentation. In *International Conference on Medical Image Computing and Computer-Assisted Intervention*, pages 370–378. Springer, 2018. 3
- [29] S. Qiao, W. Shen, Z. Zhang, B. Wang, and A. Yuille. Deep co-training for semi-supervised image recognition. *ECCV*, 2018. 1, 2, 4, 6
- [30] Z. Qiu, T. Yao, and T. Mei. Learning spatio-temporal representation with pseudo-3d residual networks. In *2017 IEEE*

International Conference on Computer Vision (ICCV), pages 5534–5542. IEEE, 2017. 8

- [31] A. Rasmus, M. Berglund, M. Honkala, H. Valpola, and T. Raiko. Semi-supervised learning with ladder networks. In *Advances in Neural Information Processing Systems*, pages 3546–3554, 2015. 2
- [32] H. R. Roth, L. Lu, A. Farag, H.-C. Shin, J. Liu, E. B. Turkbey, and R. M. Summers. Deeporgan: Multi-level deep convolutional networks for automated pancreas segmentation. In *MICCAI*, 2015. 5
- [33] H. R. Roth, L. Lu, J. Liu, J. Yao, A. Seff, K. Cherry, L. Kim, and R. M. Summers. Improving computer-aided detection using convolutional neural networks and random view aggregation. *IEEE transactions on medical imaging*, 35(5):1170–1181, 2016. 3
- [34] M. Sajjadi, M. Javanmardi, and T. Tasdizen. Regularization with stochastic transformations and perturbations for deep semi-supervised learning. In *Advances in Neural Information Processing Systems*, pages 1163–1171, 2016. 2
- [35] K. Simonyan and A. Zisserman. Very deep convolutional networks for large-scale image recognition. *arXiv preprint arXiv:1409.1556*, 2014. 1
- [36] C. Szegedy, W. Liu, Y. Jia, P. Sermanet, S. Reed, D. Anguelov, D. Erhan, V. Vanhoucke, and A. Rabinovich. Going deeper with convolutions. In *Proceedings of the IEEE conference on computer vision and pattern recognition*, pages 1–9, 2015. 1
- [37] Y. Xia, L. Xie, F. Liu, Z. Zhu, E. K. Fishman, and A. L. Yuille. Bridging the gap between 2d and 3d organ segmentation. *MICCAI*, 2018. 3
- [38] C. Xu, D. Tao, and C. Xu. A survey on multi-view learning. *arXiv preprint arXiv:1304.5634*, 2013. 2, 3
- [39] P. A. Yushkevich, J. Piven, H. Cody Hazlett, R. Gimpel Smith, S. Ho, J. C. Gee, and G. Gerig. User-guided 3D active contour segmentation of anatomical structures: Significantly improved efficiency and reliability. *Neuroimage*, 31(3):1116–1128, 2006. 11
- [40] H. Zhao, J. Shi, X. Qi, X. Wang, and J. Jia. Pyramid scene parsing network. In *IEEE Conf. on Computer Vision and Pattern Recognition (CVPR)*, pages 2881–2890, 2017. 1
- [41] Y. Zhou, Y. Wang, P. Tang, W. Shen, E. K. Fishman, and A. L. Yuille. Semi-supervised multi-organ segmentation via multi-planar co-training. *WACV*, 2019. 3, 6
- [42] Y. Zhou, L. Xie, W. Shen, Y. Wang, E. K. Fishman, and A. L. Yuille. A fixed-point model for pancreas segmentation in abdominal CT scans. In *MICCAI*, 2017. 3
- [43] Z.-H. Zhou and M. Li. Semi-supervised regression with co-training. In *IJCAI*, volume 5, pages 908–913, 2005. 2
- [44] Z.-H. Zhou and M. Li. Tri-training: Exploiting unlabeled data using three classifiers. *IEEE Transactions on knowledge and Data Engineering*, 17(11):1529–1541, 2005. 2
- [45] Z. Zhu, Y. Xia, W. Shen, E. K. Fishman, and A. L. Yuille. A 3d coarse-to-fine framework for volumetric medical image segmentation. In *3DV*, 2018. 5

A. 3D Visualizations

Here, we give additional visualizations illustrating the positive influence of UMCT on 3D segmentation with ITK-SNAP [39]. See Fig. 3 and 4.

NIH dataset (*pancreas*): Case #5

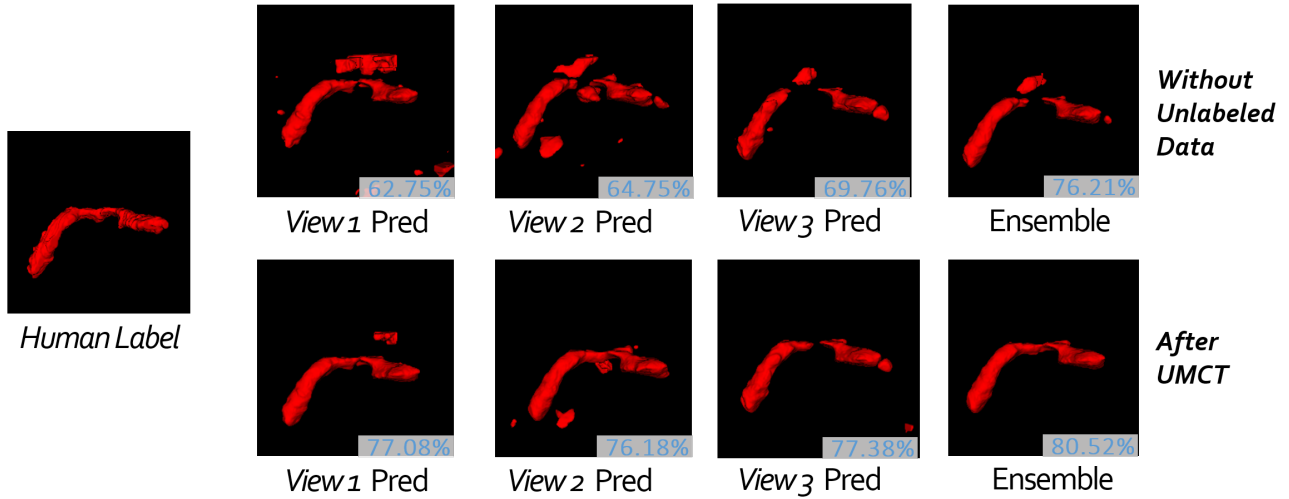


Figure 3: NIH case 5 visualization of 3D mask.

NIH dataset (*pancreas*): Case #11

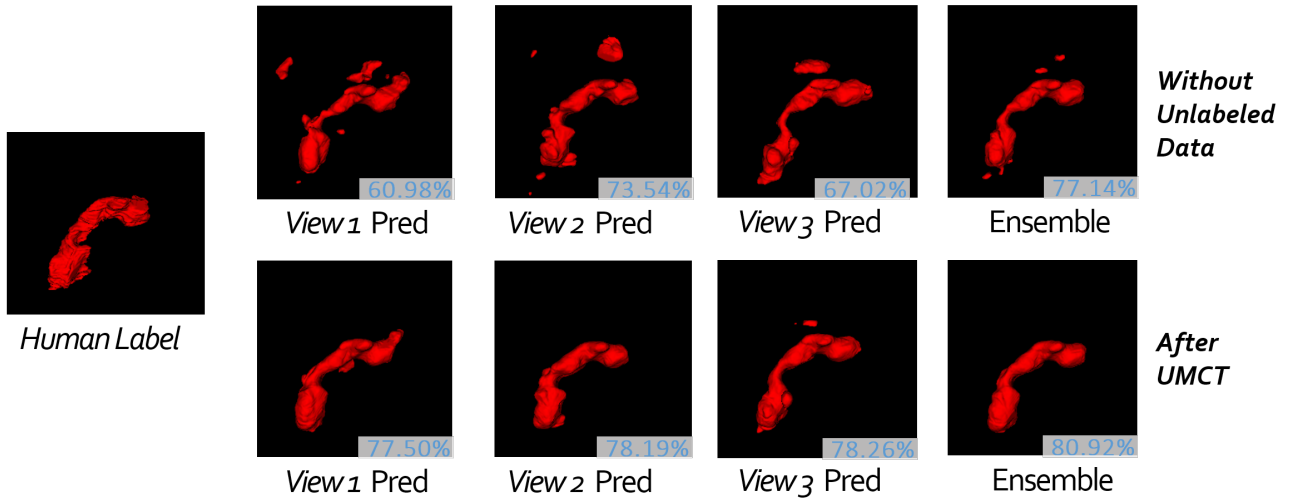


Figure 4: NIH case 11 visualization of 3D mask.